Nano-Micro Lett. (2017) 9:14
DOI 10.1007/s40820-016-0115-3

ARTICLE

# $BiVO_4/TiO_2(N_2)$ Nanotubes Heterojunction Photoanode for Highly Efficient Photoelectrocatalytic Applications

**Rui Wang[1] · Jing Bai[1] · Yunpo Li[1] · Qingyi Zeng[1] · Jinhua Li[1] · Baoxue Zhou[1,2]**

Received: 8 August 2016 / Accepted: 7 October 2016 / Published online: 9 November 2016


**Abstract** We report the development of a novel visible response $BiVO_4/TiO_2(N_2)$ nanotubes photoanode for photoelectrocatalytic applications. The nitrogen-treated $TiO_2$ nanotube shows a high carrier concentration rate, thus resulting in a high efficient charge transportation and low electron–hole recombination in the $TiO_2$–$BiVO_4$. Therefore, the $BiVO_4/TiO_2(N_2)$ NTs photoanode enabled with a significantly enhanced photocurrent of 2.73 mA $cm^{-2}$ (at 1 V vs. Ag/AgCl) and a degradation efficiency in the oxidation of dyes under visible light. Field emission scanning electron microscopy, X-ray diffractometry, energy-dispersive X-ray spectrometer, and UV–Vis absorption spectrum were conducted to characterize the photoanode and demonstrated the presence of both metal oxides as a junction composite.

**Graphical Abstract** Visible-light response $BiVO_4/TiO_2(N_2)$ naontubes photoelectrode was fabricated for photoelectrochemical water splitting and organic degradation in this paper.

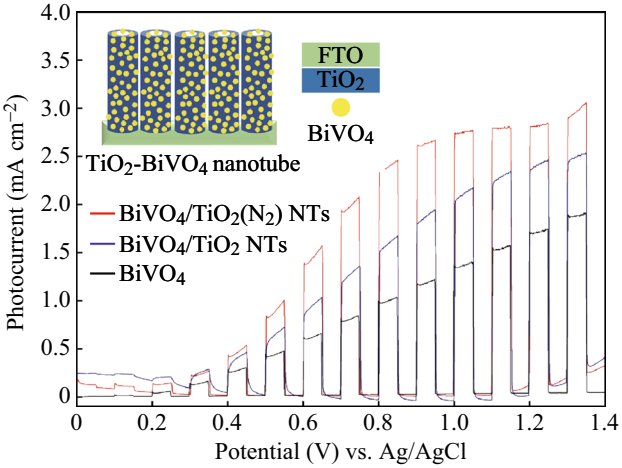


**Electronic supplementary material** The online version of this article (doi:10.1007/s40820-016-0115-3) contains supplementary material, which is available to authorized users.

✉ Jing Bai
bai_jing@sjtu.edu.cn

✉ Baoxue Zhou
zhoubaoxue@sjtu.edu.cn

[1] School of Environmental Science and Engineering, Shanghai Jiao Tong University, Shanghai 200240, People's Republic of China

[2] Key Laboratory of Thin Film and Microfabrication Technology for Ministry of Education, Shanghai 200240, People's Republic of China

**Keywords** $BiVO_4$ · $TiO_2(N_2)$ nanotube · Heterojunction · Photoelectrocatalytic · Degradation of dyes

## 1 Introduction

The extreme shortage of natural resources and severe environmental problems caused by burning fossil fuels are pressing global concerns. In the past decades, many efforts

were made to explore alternate energy sources. Photoelectrocatalytic (PEC) technology is widely recognized as an alternative energy source because it provides a highly efficient and eco-friendly route to produce renewable energy, and it degrades organic pollutants by the direct use of sunlight [1–4]. It can be achieved using a semiconductor photoanode/liquid junction, which drives an oxidation reaction. Therefore, in most PEC cells, the overall performance is primarily determined by the photoanode. However, it is still a challenge to synthesize a photoanode material that is chemically stable and has reasonably high incident light-to-current conversion efficiency in the visible range.

In recent years, $Bi^{3+}$-based complex oxides that could absorb visible light effectively and with the advantage of price beneficial have been produced as alternative energy materials [5–8]. $BiVO_4$ is a promising high efficient photoanode and photocatalysis material, with advantages of small optical band gaps (2.4 eV) and high stability, and low conduction band edges that overcome traditional photoanode materials, such as ZnO, $TiO_2$, $WO_3$, and $Fe_2O_3$ [9–13]. However, $BiVO_4$ has the shortages of poor carrier transport properties and a substantially less efficient physical photoconversion rate [8].

One approach for alleviating these limitations is to use another semiconductor as support material to form a heterojunction that not only facilitates carrier transport but also enhances light absorption. Among various semiconductors, $TiO_2$ has been intensively studied as a promising photoanode because it is stable, cost-effective, and has a negative flat band potential ($\sim$0.2 V vs. RHE) (RHE, reversible hydrogen electrode) [14–18]. Recently, Xie et al. [19] found an unusual spatial transfer of visibly excited high-energy electrons of $BiVO_4$ to $TiO_2$, which indicated enhanced photoactivity in the heterojunction of $BiVO_4$/$TiO_2$ nanoparticles. Li et al. [20] demonstrated that a proper facet contact between $BiVO_4$ and $TiO_2$ nanoparticles was the key to improving the photoactivity of $BiVO_4$. Recently, we studied one-dimensional (1D) nanostructured $TiO_2$ coupled with a $BiVO_4$ heterojunction with straight channels for electron transportation that reduced carrier diffusion lengths and improved charge collection efficiencies [21]. However, $TiO_2$ has an intrinsically low mobility that limits the enhancement of photoactivity of the $BiVO_4$–$TiO_2$ heterojunction. Therefore, increasing the carrier concentration and also the conductivity in $TiO_2$ is crucial to constructing a $BiVO_4$–$TiO_2$ heterojunction for a high-performance PEC cell.

In this study, we pre-treated $TiO_2$ nanotubes in the nitrogen gas ($TiO_2(N_2)$ NTs) and then coupled them with $BiVO_4$ to form a $BiVO_4/TiO_2(N_2)$ NTs heterojunction. We find that the photocurrent is increased by approximately 30 % compared to those obtained by previously reported $BiVO_4/TiO_2$ NTs heterojunction [21]. Our PEC experiments further demonstrate the improved performance in the degradation of dyes. These results are attributed to the high carrier concentration of $TiO_2$ NTs after annealing in a non-oxidizing atmosphere, as observed by Mott–Schottky spectra. In this case, the defects presented in the $TiO_2(N_2)$ NTs increase the charge transfer kinetics, along with the reduced recombination losses due to trap filling. Thus, the charge transport between $BiVO_4$ and $TiO_2$ is enhanced to produce a higher photoactivity. This heterojunction provides useful insight into the design and fabrication of $BiVO_4$-based photoanodes for potentially cost-effective and highly efficient PEC applications in large-scale applications.

## 2 Experimental Procedures

### 2.1 Preparation of $BiVO_4/TiO_2(N_2)$ NTs Photoanodes

$TiO_2$ NTs were prepared by a template method in which ZnO nanowires (NWs) were transformed during a liquid-phase deposition (LPD) process. ZnO NWs were synthesized on FTO glass ($2 \times 2$ $cm^2$) after a hydrothermal treatment [22]. Next, a LPD treatment was conducted by placing ZnO NW substrates in a mixed solution of 50 mm $(NH_4)_2TiF_6$ and 150 mm $H_3BO_3$ for 20 min at 25 °C [23]. After the LPD treatment, the sample was further annealed at 500 °C for 2 h in nitrogen gas, and nitrogen-treated $TiO_2$ NTs were obtained and marked as $TiO_2(N_2)$ NTs. For the fabrication of the $BiVO_4/TiO_2(N_2)$ NTs photoanode, a yellow precursor solutions of 300 mM $Bi(NO_3)_3$ and 300 mM $NH_4VO_3$ in 2 M $HNO_3$ were deposited on the $TiO_2$ NTs by spin coating [24]. Finally, the samples were sintered at 450 °C for 2 h in room air and yielded a yellow $BiVO_4/TiO_2(N_2)$ NTs film. For the control, the $TiO_2$ NTs annealed in room air were used to prepare the $BiVO_4/TiO_2$ NTs photoanodes and bare $BiVO_4$/FTO photoanodes were also prepared using the same procedure without the $TiO_2$ NTs substrate.

### 2.2 Structural Characterization

The morphologies of the samples were characterized using field emission scanning electron microscopy and a microscope equipped with an energy-dispersive X-ray spectrometer (EDX) (FEI, Sirion200) and TEM (JEM-2100F, JEOL, Japan). The crystalline phase of the samples was characterized by X-ray diffractometry (XRD) (AXS-8 Advance, Bruker, Germany). X-ray photoelectron spectroscopy (XPS) measurements were performed on an ESCALAB250 XPS measuring system with a Mg Kα

X-ray source. Optical absorption measurements were conducted in a Lamda 750 UV–Vis–IR spectrophotometer using an integrating sphere.

### 2.3 Photoelectrochemical Measurements

The photo responses of the $BiVO_4/TiO_2$ NTs photoanode were conducted using a three-electrode system with the Ag/AgCl electrode as the reference, platinum foil as the auxiliary electrode, and the samples as the working electrode. The working electrode potential and current were controlled by an electrochemical workstation (CHI 660c, CH Instruments Inc., TX, USA). A 350-W Xe lamp was used as a simulated light source, without further description, and all experiments were conducted under visible light (light intensity, 100 mW $cm^{-2}$). The electrolyte was a 0.1 M $Na_2SO_4$ solution. The linear sweep voltammograms (LSV) were conducted under chopped light irradiation. The scan rate for the linear sweep voltammetry was 10 mV $s^{-1}$. Photoluminescence (PL) measurements were conducted using an OmniPL-LF325 system with a 325 nm laser at room temperature. The incident photon-to-charge conversion efficiency (IPCE) was measured by a system comprising a monochromator (Zolix, P.R. China), a 500-W xenon arc lamp, a calibrated silicon photodetector, and a power meter. Mott–Schottky (impedance) spectra were recorded in 0.2 M $Na_2SO_4$ without light at a frequency of 1 kHz and a scan rate of 10 mV $s^{-1}$.

Intensity modulated photocurrent spectroscopy (IMPs) was determined using an electrochemical workstation (ZENNIUM, ZAHNER-elecktrik GmbH & Co. KG, Germany) equipped with a controlled intensity modulated photospectroscopy setup (CIMPS, PP211, ZAHNER-elecktrik GmbH & Co. KG, Germany) after a two-electrode configuration. A white light lamp (WLC02, ZAHNER-elecktrik GmbH & Co. KG, Germany) was used as the light source. The modulated light in the frequency range of 0.1 Hz–1 kHz superimposed on a steady dc light with an intensity of 60 mW $cm^{-2}$ was also used as a light source.

### 2.4 Organics Compounds Degradation

The PEC degradation of the methylene blue (MB) experiment was conducted under the following conditions: visible light irradiation (100 mW $cm^{-2}$), vigorous stirring, 1.0 V (vs. Ag/AgCl) of electric bias, pH 7, and 0.1 M sodium sulfate as the supporting electrolyte. Before degradation test, the nitrogen was bubbled to remove oxygen from the solution. The initial concentration of MB solution was 10 mg $L^{-1}$ and the reaction solution was 20 mL during the experiment. The degradation rates of the dyes were analyzed with an UV–Vis spectrophotometer (UV2102 PCS, UNICO, Shanghai).

## 3 Results and Discussion

The main fabrication strategies for the $BiVO_4/TiO_2(N_2)$ NTs photoanodes are conducted in three steps as illustrated in Fig. 1. First, the ZnO NW template is grown on the FTO substrate through a hydrothermal method. Second, the template is transformed to $TiO_2$ NTs after an LPD treatment which involves hydrolysis of ammonium hexafluorotitanate, and leads to the deposition of $TiO_2$ as well as mild etching of ZnO from the formation of HF. Third, $BiVO_4$ is deposited on the $TiO_2$ NTs to form a photoactive composite layer.

Figure 2 shows the top and cross-sectional SEM images of optimized $TiO_2(N_2)$ NTs and $BiVO_4/TiO_2(N_2)$ NTs, respectively. As shown in Fig. 2a, b, the obtained $TiO_2(N_2)$ NTs have a vertical geometric shape, although the treatment of the NWs leads to partial connectivity among the constituent wires due to the surface tension during the evaporation of the solvent (Fig. 2a). Compared with the nitrogen-treated $TiO_2$ NTs, the geometry for the air-annealed $TiO_2$ NTs remains unchanged (not presented here). The $TiO_2$ NTs are approximately 400 nm in length with a relatively rough surface (Fig. 2b). The top view SEM images of the $BiVO_4/TiO_2(N_2)$ NTs reveal that the $TiO_2(N_2)$ NTs are completely covered by $BiVO_4$ (Fig. 2c). Likewise, the side view also confirms the formation of the heterojunction of the $BiVO_4/TiO_2(N_2)$ NTs heterojunction (Fig. 2d). The thickness of the junction is approximately 600 nm, which is thicker than that of pure $BiVO_4$ photoanode (Fig. S1). As shown in Fig. S2, the TEM images also demonstrate the heterojunction structure, where the $BiVO_4$ nanoparticles are clearly observed on the $TiO_2$ NTs.

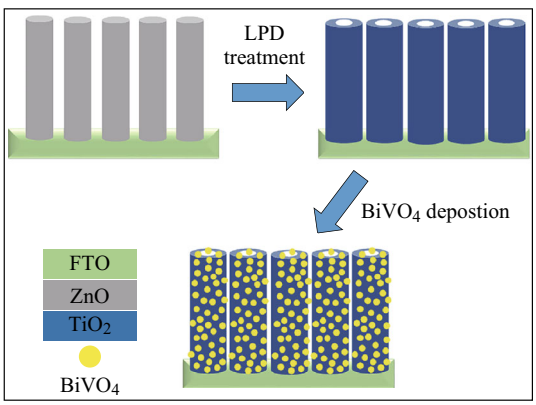


**Fig. 1** Schematic diagram of the main processes for the fabrication of the $BiVO_4/TiO_2$ NTs photoanodes

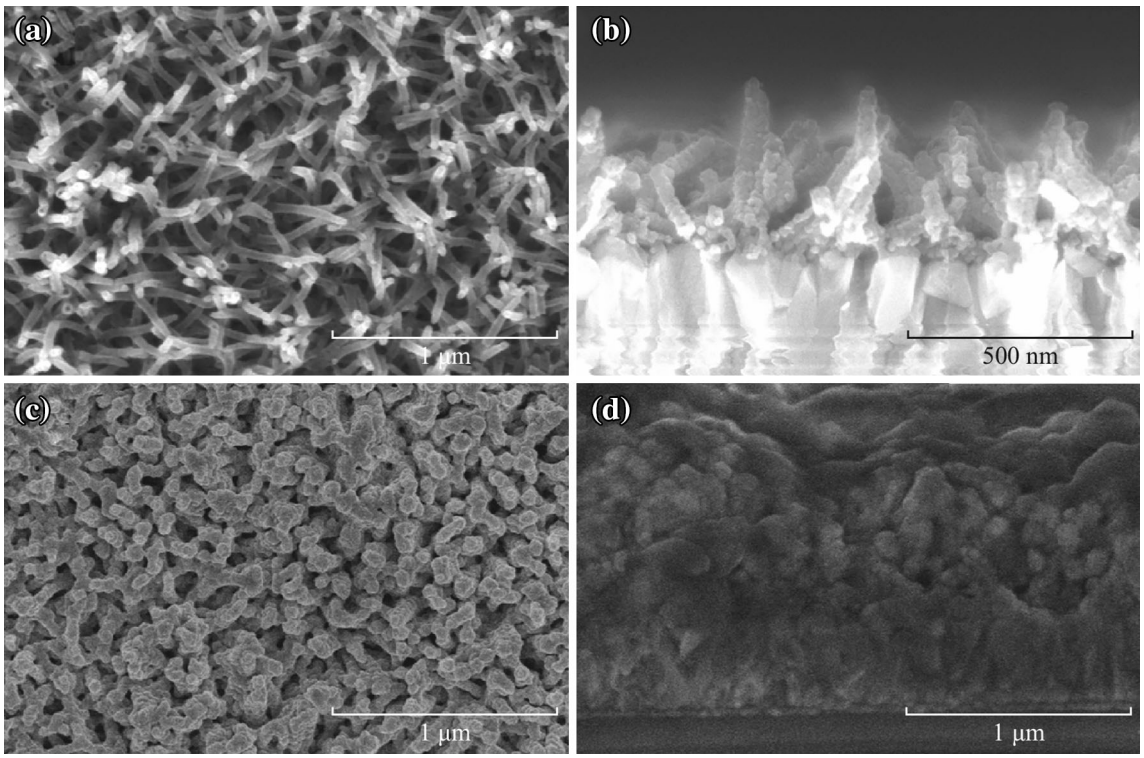


**Fig. 2** Top view and cross-sectional SEM images of $TiO_2(N_2)$ NTs (**a**, **b**), and $BiVO_4/TiO_2(N_2)$ NTs (**c**, **d**)

The elemental composition of the $BiVO_4/TiO_2(N_2)$ NTs was also analyzed and their characteristic elements were identified using an EDX detection spectrometer. As shown in Fig. S2, the elements of Bi and V have almost the same percentage of atoms (%), indicating the formation of $BiVO_4$. XRD also measured the crystalline phases of $BiVO_4$ and $BiVO_4/TiO_2$ NTs, and the results are shown in Fig. 3. For all samples, the prominent peaks for $BiVO_4$ are likely derived from the monoclinic phase of $BiVO_4$ (PDF 14-0688). The typical peaks at 25.3° and 27.4° are assigned

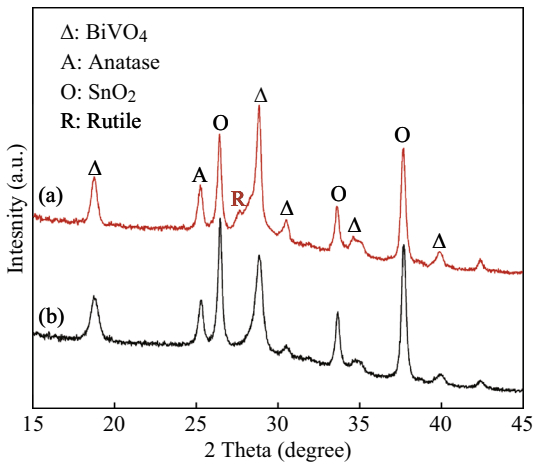


**Fig. 3** XRD patterns of **a** $BiVO_4/TiO_2$ NT and **b** the $BiVO_4/TiO_2(N_2)$ NTs electrode

to the (101) and (110) planes of anatase and rutile phases, respectively. In Fig. 3a, the annealed composite has anatase phase and a large amount of rutile phase from the integrated intensity of the peaks associated with the (101) and (110) planes. However, for the $BiVO_4/TiO_2(N_2)$ NTs sample, it contains mostly anatase (Fig. 3b). These results are in accord with the reports by Jin et al. [25] and Mahajan et al. [26], who studied the effects of the atmosphere on the crystalline phase of $TiO_2$ nanotube arrays in the annealing process. Also, the peaks at 26.4° and 37.6° for both samples are ascribed to the FTO substrate. To further study the surface composition and chemical state of $TiO_2(N_2)$, XPS analysis was also conducted, and the results are illustrated in Fig. 4. The full survey indicates the presence of Sn, O, Ti, and N (Fig. 4a). Figure 4b–d shows the high-resolution XPS spectra of the elements, respectively. For the O 1s (Fig. 4b), the peak at 531.0 eV corresponds to the lattice oxygen, which is related to the Ti–O or Sn–O chemical bonding in the $SnO_2$ or $TiO_2$. Two distinct peaks located at 464.5 and 458.7 eV in Fig. 4c are assigned to the binding energy of Ti $2p_{1/2}$ and Ti $2p_{3/2}$, respectively, indicating the presence of $Ti^{3+}$. The peak at 400.1 eV could ascribe to γ-N state, which is molecularly chemisorbed $N_2$ [27].

The optical absorption spectra of the $TiO_2$ NTs, $TiO_2(N_2)$ NTs, $BiVO_4/TiO_2$ NTs, and the $BiVO_4/TiO_2(N_2)$ NTs are shown in Fig. 5. The $TiO_2$ NTs show an absorption edge at ~360 nm, whereas, the $TiO_2(N_2)$ NTs with an

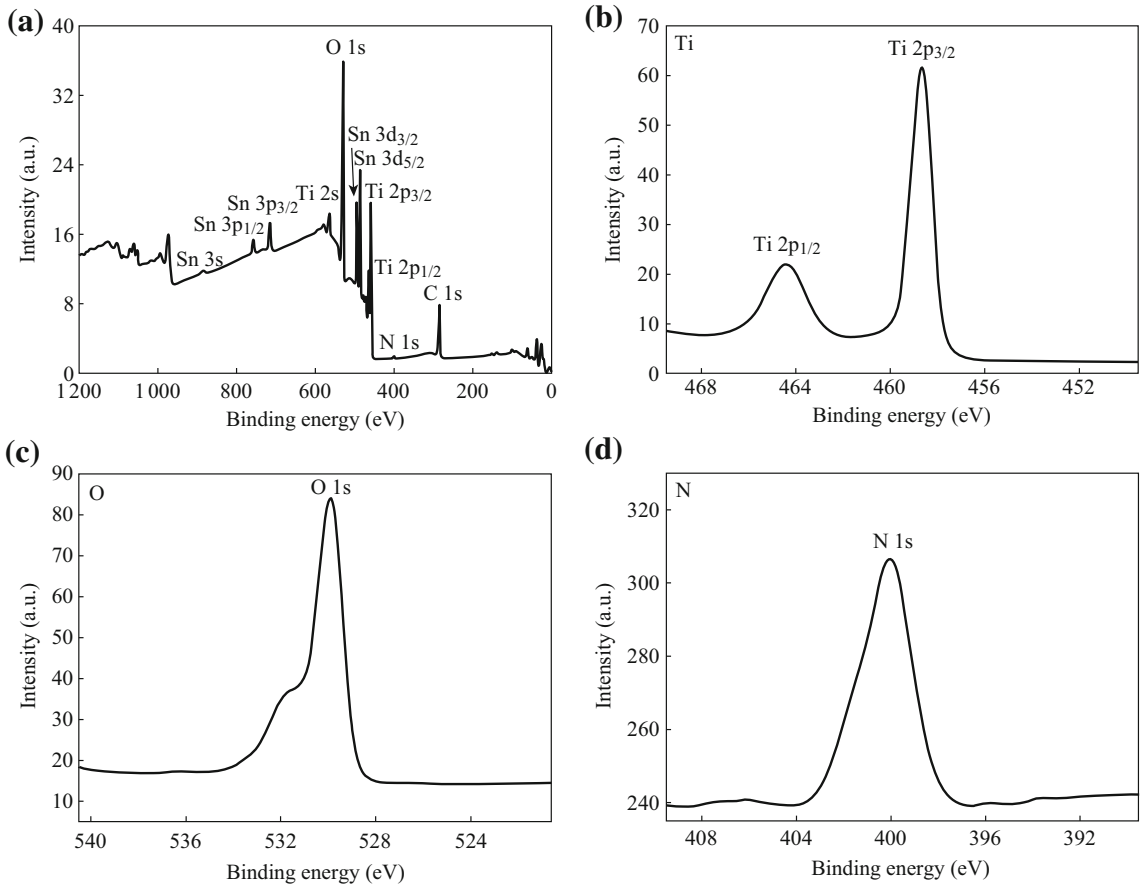


**Fig. 4** **a** X-ray photoelectron spectroscopy survey scan over a large energy range at low-resolution and high-resolution Ti 2p, **b** O 1s, **c** N 1s, **d** XPS spectra for $TiO_2(N_2)$ NTs

absorption tails extend into the visible wavelength regions. The long absorption tail indicates the presence of additional energy states within the band gap of $TiO_2$. The energy may have resulted from the presence of oxygen vacancies or non-stoichiometric $TiO_2$ due to annealing in a non-oxidizing atmosphere. On the other hand, the pure $BiVO_4$ film displayed absorption within the visible region of the spectrum with the edge at ~516 nm, which corresponded to the band gap energy of 2.4 eV and further demonstrated the formation of monoclinic phase $BiVO_4$ [28]. After the deposition of $BiVO_4$, both the $BiVO_4/TiO_2$ NTs and the $BiVO_4/TiO_2(N_2)$ NTs had very similar band gap absorption compared to $BiVO_4$, although they had enhanced intensities in the visible region. The enhanced absorption intensity was attributed to the thicker $BiVO_4$ film in the heterojunction as observed in the SEM images.

Figure 6 presents the LSV characteristics of the $TiO_2$ NTs, $TiO_2(N_2)$ NTs, $BiVO_4$,$BiVO_4/TiO_2$NTs, and the $BiVO_4/TiO_2(N_2)$NTs, respectively. The $TiO_2$ NTs sample exhibited a pretty low photocurrent under visible irradiation due to its large band gap, whereas the $TiO_2(N_2)$ NTs sample had a slight photocurrent. The photocurrent for pure $BiVO_4$ increased steadily with the increasing potential of the working electrode, and a photocurrent density of 1.36 mA $cm^{-2}$ (1.0 V vs. Ag/AgCl) was obtained. Compared to that of pure $BiVO_4$, a significant enhancement in photocurrent, ca. 2.06 mA $cm^{-2}$ (1.0 V vs. Ag/AgCl), by the $BiVO_4/TiO_2$ NTs was observed. The photocurrent was further enhanced by approximately 30 % when using the $BiVO_4/TiO_2(N_2)$ NTs, which obtained the photocurrent of 2.73 mA $cm^{-2}$ (1.0 V vs. Ag/AgCl). The $BiVO_4/TiO_2(N_2)$ with the cyclic voltammetry test also shows a stable photocurrent in the measuring range (Fig. S4).

Incident photon-to-current efficiency was measured in order to ascertain the light conversion efficiency of heterojunction of the $BiVO_4/TiO_2(N_2)$ NTs and was compared to the $BiVO_4/TiO_2$ NTs, $BiVO_4$, and $TiO_2$ in Fig. 6b. Due to a large band gap, both the $TiO_2$ NTs and $TiO_2(N_2)$ NTs had low efficiencies below 400 nm, although the $TiO_2(N_2)$ NTs exhibited better performances. The IPCE of $BiVO_4$ was comparatively at ~20 % at 410 nm, whereas heterojunction $BiVO_4/TiO_2$ NTs had a higher IPCE at nearly 28 % at 410 nm. Comparably, the IPCE of $BiVO_4/TiO_2(N_2)$ NTs further increased to 44 % at 410 nm, which

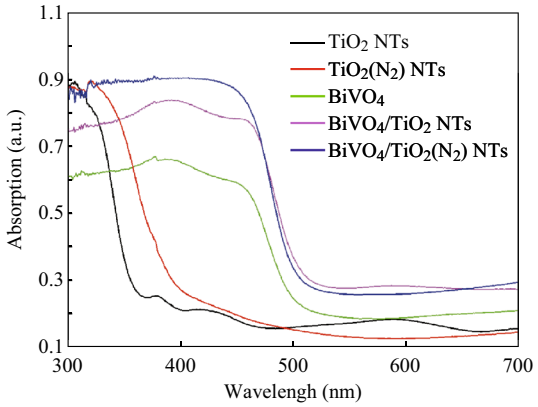


**Fig. 5** Photo-absorption spectra of the $TiO_2$ NTs, $TiO_2(N_2)$ NTs, $BiVO_4$, $BiVO_4/TiO_2$ NTs, and the $BiVO_4/TiO_2(N_2)$ NTs, respectively

was more than 100 % higher than the IPCE of bare $BiVO_4$. This again suggests that the rectifying electron transfer from $BiVO_4$ to $TiO_2$ likely inhibits the fast recombination and increases the solar energy conversion efficiency of the junction. The IPCE was nearly zero at 550 nm, which is consistent with the optical absorption of the samples.

The PEC properties of the $BiVO_4/TiO_2(N_2)$ NTs were investigated by treating the organic dye (MB) under visible light illumination. It can be seen that almost no MB or little MB can be directly degraded by only applying electrocatalytic or photolytic reaction, and the $TiO_2$ NTs only resulted in a removal ratio of only 14.1 % within 80 min, whereas the $TiO_2(N_2)$ NTs had a higher efficiency of 27.2 % under the same conditions. The limited improvement in degradation of MB by $TiO_2$ NTs was due to a large band gap that limited the use of visible light. Compared to the $TiO_2$ NTs, the $BiVO_4$ electrode degraded 52.4 % of the MB within the same time because of good absorption in the visible region. For the $BiVO_4/TiO_2$ NTs, the removal rate increased to 76.7 % due to fast electron transfers between the $BiVO_4$ and $TiO_2$ NTs. However, it is easily observed from Fig. 7a that the $BiVO_4/TiO_2(N_2)$ NTs obtained the removal rate of 91.8 % under the same conditions. The recycle performance of the $BiVO_4/TiO_2(N_2)$ NTs for PEC degradation of MB was investigated in five PEC cycles, and the results are shown in Fig. 7b. These results further suggested that the $BiVO_4/TiO_2$ NTs were stable for PEC applications, such as treating organic wastewater [29–31]. During all the process in PEC, we use 1 $cm^2$ photoanode under visible light illumination to react.

As previously discussed, the $BiVO_4/TiO_2(N_2)$ NTs exhibited a significant enhancement in photoactivity as verified by higher photocurrent as well as a higher PEC efficiency in the degradation of dyes. Apparently, the $TiO_2(N_2)$ NTs played an important role in the promotion of the charge transfers in the electrode. We concluded that the carrier concentration in the $TiO_2$ NTs could be increased after annealing in a nitrogen atmosphere. To make sure the impacts of the $TiO_2(N_2)$ NTs, impedance measurements were carried out at a frequency of 1 kHz on both the $TiO_2(N_2)$ NTs and $TiO_2$ NTs electrodes in 0.2 M $Na_2SO_4$ electrolytes in the dark. The results are demonstrated by the Mott–Schottky plots in Fig. 8a. From the linear portion of the Mott–Schottky plots, charge carrier densities are calculated using the relation

$$N_D = \frac{2}{e\varepsilon\varepsilon_0 m'} \quad (1)$$

where $N_D$ is the charge carrier density, $e$ is the elementary electron charge ($e = 1.6 \times 10^{-19}$ C), $\varepsilon$ is the dielectric constant ($\varepsilon = 48$), $\varepsilon_0$ is the permittivity in vacuum ($\varepsilon_0 = 8.85 \times 10^{-12}$ F $m^{-1}$), and $m$ is the slope of the $1/C^2$ versus potential plot. A charge carrier density of $2.9 \times 10^{18}$ $cm^{-3}$ was determined for the $TiO_2$ NTs, but was $2.1 \times 10^{19}$ $cm^{-3}$ for the $TiO_2(N_2)$ NTs. These results indicated that the charge carrier concentration of the $TiO_2$

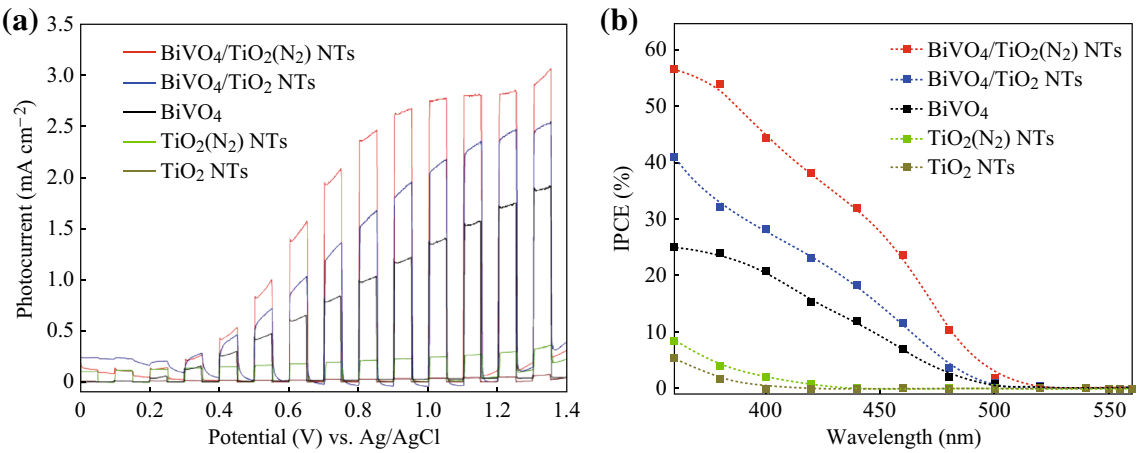


**Fig. 6** **a** Photoelectrochemical responses of the $TiO_2$ NTs, $TiO_2(N_2)$ NTs, $BiVO_4$, $BiVO_4/TiO_2$ NTs, and the $BiVO_4/TiO_2(N_2)$ NTs under illumination of chopped visible irradiation in 0.1 M $Na_2SO_4$ solution and **b** corresponding IPCE spectra

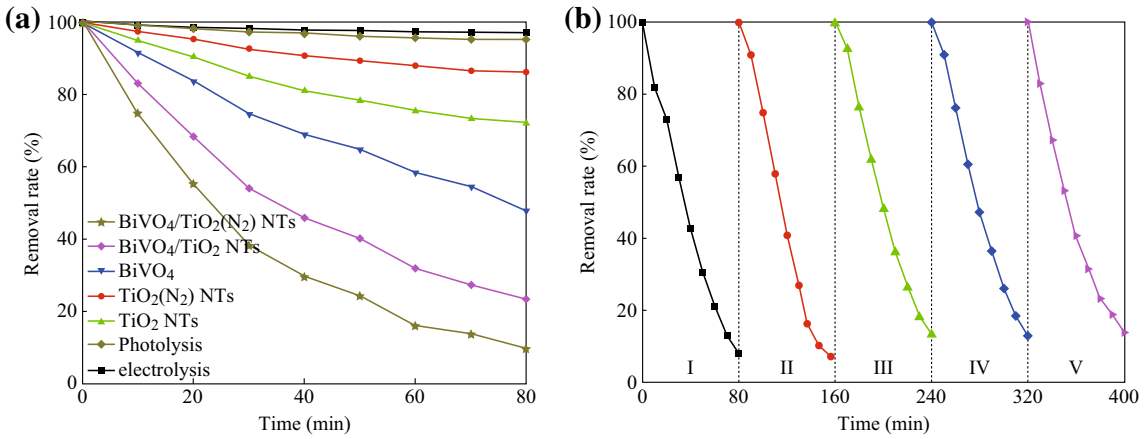


**Fig. 7** **a** PEC degradation of MB using different photoanodes under visible light illumination and **b** stability of $BiVO_4/TiO_2(N_2)$ NTs photoanodes for degradation of MB during a series of five identical tests

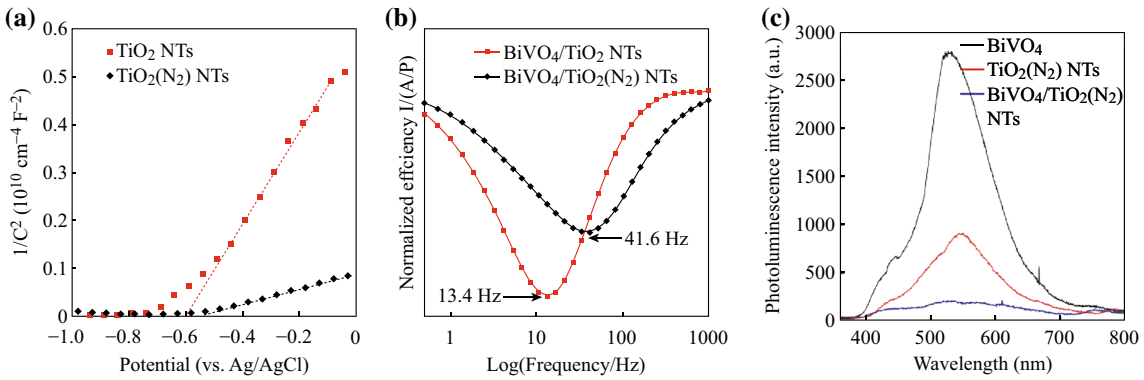


**Fig. 8** **a** Mott–Schottky plots for the $TiO_2$ NTs and $TiO_2(N_2)$ NTs electrodes measured in 0.2 M $Na_2SO_4$ at 1 kHz and **b** IMPS for $BiVO_4/TiO_2$ NTs and $BiVO_4/TiO_2(N_2)$ NTs, **c** PL spectra for $BiVO_4$, $TiO_2(N_2)$ NTs, and $BiVO_4/TiO_2(N_2)$ NTs

NTs was indeed increased after calcination in the non-oxidizing atmospheres. The higher defect density of the nitrogen-annealed sample also involved a higher electrical conductivity [32] and rapid charge transfer.

To further confirm enhanced charge transfers between $BiVO_4$ and the $TiO_2(N_2)$ NTs in the heterojunction material, the transit time ($\tau_d$) of the majority carriers in the $BiVO_4/TiO_2$ NTs electrode and the $BiVO_4/TiO_2(N_2)$ NTs electrode was measured by IMPS, respectively. The transit time $\tau_d$ was the average time that the photogenerated charges took to transfer to the back contact, and were estimated from the equation $\tau_d = (2\pi \cdot f_{min}\ (\text{IMPS}))^{-1}$, where $f_{min}$ is the frequency at the minimal value in the IMPS plot. The transit time reflects the recombination probability of the photogenerated electrons and holes in the photoelectrode [33]. Figure 8b shows the IMPS plots of the $BiVO_4/TiO_2$ NTs electrode and the $BiVO_4/TiO_2(N_2)$ NTs electrode, respectively. According to the previous equation, the transit time $\tau_d$ for the $BiVO_4/TiO_2$ NTs was 11.9, and 3.82 ms for $BiVO_4/TiO_2(N_2)$ NTs electrode, which indicated that the transport speed of the majority of photogenerated charges in the $BiVO_4/TiO_2(N_2)$ NTs electrode was three times faster than that of the $BiVO_4/TiO_2$ electrode. In other words, the $BiVO_4/TiO_2(N_2)$ NTs heterojunction could facilitate the majority of the photogenerated charges transported to the counter electrode and likewise, the transport of photogenerated electrons to the electrolyte is enhanced.

The transportation of electrons between the two materials was also certified by PL measurement as shown in Fig. 8c. We observed strong emission from bare $TiO_2$ NTs and $BiVO_4$, whereas the $BiVO_4/TiO_2$ heterojunction resulted in a near 90 % reduction in the emission intensity. The obvious quenching of luminescence of $BiVO_4$ is characteristic of charge transfer between the $BiVO_4$ and $TiO_2$ NTs, implying a strong indication of the efficient reduction in recombination of charge carriers in the 1D heterojunction material. In consequence, the separation efficiency of photogenerated electron–hole pairs in $BiVO_4/TiO_2(N_2)$ NTs heterojunction could be improved.

Based on the experiments, We concluded that the improved performance of the $BiVO_4/TiO_2(N_2)$ NTs was

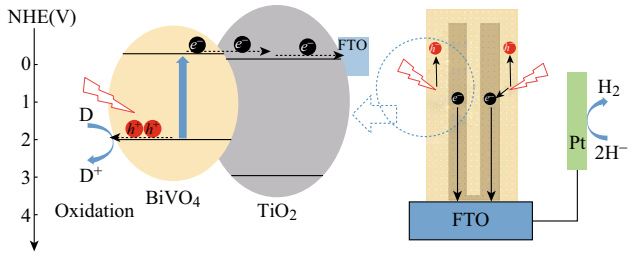


**Fig. 9** Schematic of energy bands and charge transfers at $BiVO_4$/$TiO_2(N_2)$ NTs photoanodes

primarily due to enhanced optical absorption and specific $TiO_2(N_2)$ NTs. The nanotube structure provides larger surface area than the planar structure so that more $BiVO_4$ photocatalyst was loaded for absorbing more visible light. On the other hand, the presence of oxygen vacancies or non-stoichiometric $TiO_2$ in the $TiO_2(N_2)$ NTs significantly enhanced the carrier density which favors the separation of photo-introduced electron–hole pairs verified by IMPS test. Thus, the higher photocurrent was obtained. The whole PEC system is shown in Fig. 9. Upon excitation by visible light, electrons were photoexcited from the valence band of $BiVO_4$ to its conduction band. Then electron differences in the positions of the conduction bands which drove to photoelectrons generated in $BiVO_4$ to the tubular $TiO_2(N_2)$ NTs, where electrons were rapidly separated and directed to the Pt counter electrode via the external circuit. Consequently, the photogenerated electrons were scavenged by hydrogen ions on the Pt foil, and formed hydrogen gas, while the photogenerated holes oxidized water or organics on the surface of the $BiVO_4$. Overall, the $BiVO_4/TiO_2(N_2)$ NTs heterojunction offered remarkable photoconversion efficiency.

## 4 Conclusions

A visible light response $BiVO_4/TiO_2(N_2)$ NTs photoelectrode was fabricated for photoelectrochemical (PEC) organic degradation. Mott–Schottky plots and IMPS demonstrated the increased carrier concentration in the $TiO_2(N_2)$ NTs, which enhanced electron transfers between $BiVO_4$ and $TiO_2$. A photoelectrochemical measurement confirmed that the photocurrent was increased approximately 100 % using the heterojunction when compared to bare $BiVO_4$ under 100 mW $cm^{-2}$ visible light illumination. Due to its excellent photoactivity and stability, the $BiVO_4/TiO_2(N_2)$ NTs show a promising future in PEC applications.

**Acknowledgments** The authors would like to acknowledge the National Nature Science Foundation of China (21507085, 21576162) and Shanghai Sailing Program of China (14YF1401500) for financial support.



## References

1. M.G. Walter, E.L. Warren, J.R. McKone, S.W. Boettcher, Q.X. Mi, E.A. Santori, N.S. Lewis, Solar water splitting cells. Chem. Rev. **110**(11), 6446–6473 (2010). doi:10.1021/cr1002326
2. J. Bai, J.H. Li, Y.B. Liu, B.X. Zhou, W.M. Cai, A new glass substrate photoelectrocatalytic electrode for efficient visible-light hydrogen production: CdS sensitized $TiO_2$ nanotube arrays. Appl. Catal. B **95**(3–4), 408–413 (2010). doi:10.1016/j.apcatb.2010.01.020
3. Z. Liu, X. Zhang, S. Nishimoto, M. Jin, D.A. Tryk, T. Murakami, A. Fujishima, Highly ordered $TiO_2$ nanotube arrays with controllable length for photoelectrocatalytic degradation of phenol. J. Phys. Chem. C **112**(1), 253–259 (2008). doi:10.1021/jp0772732
4. J. Bai, Y.B. Liu, J.H. Li, B.X. Zhou, Q. Zheng, W.M. Cal, A novel thin-layer photoelectrocatalytic (PEC) reactor with double-faced titania nanotube arrays electrode for effective degradation of tetracycline. Appl. Catal. B **98**(3–4), 154–160 (2010). doi:10.1016/j.apcatb.2010.05.024
5. J.W. Tang, Z.G. Zou, J.H. Ye, Efficient photocatalytic decomposition of organic contaminants over $CaBi_2O_4$ under visible-light irradiation. Angew. Chem. Int. Ed. **43**(34), 4463–4466 (2004). doi:10.1002/anie.200353594
6. Z.G. Zou, H. Arakawa, Direct water splitting into $H_2$ and $O_2$ under visible light irradiation with a new series of mixed oxide semiconductor photocatalysts. J. Photochem. Photobiol. A **158**(2–3), 145–162 (2003). doi:10.1016/S1010-6030(03)00029-7
7. A. Kudo, Photocatalyst materials for water splitting. Catal. Surv. Asia **7**(1), 31–38 (2003). doi:10.1023/A:1023480507710
8. Y. Park, K.J. McDonald, K.S. Choi, Progress in bismuth vanadate photoanodes for use in solar water oxidation. Chem. Soc. Rev. **42**(6), 2321–2337 (2013). doi:10.1039/C2CS35260E
9. Y.B. Kuang, Q.X. Jia, H. Nishiyama, T. Yamada, A. Kudo, K. Domen, A front-illuminated nanostructured transparent $BiVO_4$ photoanode for >2% efficient water splitting. Adv. Energy Mater. **6**(2), 1501645 (2016). doi:10.1002/aenm.201501645
10. S.M. Thalluri, S. Hernandez, S. Bensaid, G. Saracco, N. Russo, Green-synthesized W- and Mo-doped BiVO4 oriented along the 040 facet with enhanced activity for the sun-driven water oxidation. Appl. Catal. B **180**, 630–636 (2016). doi:10.1016/j.apcatb.2015.07.029
11. T.W. Kim, K.S. Choi, Nanoporous $BiVO_4$ photoanodes with dual-layer oxygen evolution catalysts for solar water splitting. Science **343**(6174), 990–994 (2014). doi:10.1126/science.1246913
12. L. Zhang, D.R. Chen, X.L. Jiao, Monoclinic structured $BiVO_4$ nanosheets: hydrothermal preparation, formation mechanism, and coloristic and photocatalytic properties. J. Phys. Chem. B **110**(6), 2668–2673 (2006). doi:10.1021/jp056367d
13. Y. Hu, D.Z. Li, Y. Zheng, W. Chen, Y.H. He, Y. Shao, X.Z. Fu, G.C. Xiao, $BiVO_4/TiO_2$ nanocrystalline heterostructure: a wide spectrum responsive photocatalyst towards the highly efficient decomposition of gaseous benzene. Appl. Catal. B **104**(1–2), 30–36 (2011). doi:10.1016/j.apcatb.2011.02.031
14. J. Bai, B.X. Zhou, Titanium dioxide nanomaterials for sensor applications. Chem. Rev. **114**(19), 10131–10176 (2014). doi:10.1021/cr400625j

15. X.Z. Lan, J. Bai, S. Masala, S.M. Thon, Y. Ren et al., Self-Assembled, nanowire network electrodes for depleted bulk heterojunction solar cells. Adv. Mater. **25**(12), 1769–1773 (2013). doi:10.1002/adma.201203759
16. B. Gao, Y.J. Kim, A.K. Chakraborty, W.I. Lee, Efficient decomposition of organic compounds with $FeTiO_3/TiO_2$ heterojunction under visible light irradiation. Appl. Catal. B **83**(3–4), 202–207 (2008). doi:10.1016/j.apcatb.2008.02.017
17. K. Sridharan, E. Jang, T.J. Park, Novel visible light active graphitic $C_3N_4$–$TiO_2$ composite photocatalyst: synergistic synthesis, growth and photocatalytic treatment of hazardous pollutants. Appl. Catal. B **142**, 718–728 (2013). doi:10.1016/j.apcatb.2013.05.077
18. Y. Liu, H. Zhou, J. Li, H. Chen, D. Li, B. Zhou, W. Cai, Enhanced photoelectrochemical properties of $Cu_2O$-loaded short $TiO_2$ nanotube array electrode prepared by sonoelectrochemical deposition. Nano-Micro Lett. **2**(4), 277–284 (2010). doi:10.3786/nml.v2i4.p277-284
19. M.Z. Xie, X.D. Fu, L.Q. Jing, P. Luan, Y.J. Feng, H.G. Fu, Long-lived, visible-light-excited charge carriers of $TiO_2/BiVO_4$ nanocomposites and their unexpected photoactivity for water splitting. Adv. Energy Mater. **4**(5), 1300995 (2014). doi:10.1002/aenm.201300995
20. H.F. Li, H.T. Yu, X. Quan, S. Chen, H.M. Zhao, Improved photocatalytic performance of heterojunction by controlling the contact facet: high electron transfer capacity between $TiO_2$ and the 110 facet of $BiVO_4$ caused by suitable energy band alignment. Adv. Funct. Mater. **25**(20), 3074–3080 (2015). doi:10.1002/adfm.201500521
21. J. Bai, R. Wang, Y.P. Li, Y.Y. Tang, Q.Y. Zeng et al., A solar light driven dual photoelectrode photocatalytic fuel cell (PFC) for simultaneous wastewater treatment and electricity generation. J. Hazard. Mater. **311**, 51–62 (2016). doi:10.1016/j.jhazmat.2016.02.052
22. L.E. Greene, M. Law, J. Goldberger, F. Kim, J.C. Johnson, Y.F. Zhang, R.J. Saykally, P.D. Yang, Low-temperature wafer-scale production of ZnO nanowire arrays. Angew. Chem. Int. Ed. **42**(26), 3031–3034 (2003). doi:10.1002/anie.200351461
23. J.H. Lee, I.C. Leu, M.C. Hsu, Y.W. Chung, M.H. Hon, Fabrication of aligned $TiO_2$ nanostructured arrays using a one-step templating solution approach. J. Phys. Chem. B **109**(27), 13056–13059 (2005). doi:10.1021/jp052203l
24. Q.X. Jia, K. Iwashina, A. Kudo, Facile fabrication of an efficient $BiVO_4$ thin film electrode for water splitting under visible light irradiation. Proc. Natl. Acad. Sci. **109**(29), 11564–11569 (2012). doi:10.1073/pnas.1204623109
25. V.K. Mahajan, M. Misra, K.S. Raja, S.K. Mohapatra, Self-organized $TiO_2$ nanotubular arrays for photoelectrochemical hydrogen generation: effect of crystallization and defect structures. J. Phys. D **41**(12), 125307 (2008). doi:10.1088/0022-3727/41/12/125307
26. C. Jin, W.G. Zhang, S.W. Yao, H.Z. Wang, Effect of heat-treatment process on the structure and photoelectric performance of $TiO_2$ nanotube arrays. J. Inorg. Mater. **27**(1), 54–58 (2012). doi:10.3724/SP.J.1077.2012.00054
27. R.P. Vitiello, J.M. Macak, A. Ghicov, H. Tsuchiya, L.F.P. Dick, N-doping of anodic $TiO_2$ nanotubes using heat treatment in ammonia. Electrochem. Commun. **8**(4), 544–548 (2006). doi:10.1016/j.elecom.2006.01.023
28. A. Iwase, A. Kudo, Photoelectrochemical water splitting using visible-light-responsive $BiVO_4$ fine particles prepared in an aqueous acetic acid solution. J. Mater. Chem. **20**(35), 7536–7542 (2010). doi:10.1039/c0jm00961j
29. C. Liu, Y. Ding, W. Wu, Y. Teng, A simple and effective strategy to fast remove chromium (VI) and organic pollutant in photoelectrocatalytic process at low voltage. Chem. Eng. J. **306**, 22–30 (2016). doi:10.1016/j.cej.2016.07.043
30. X. Zhao, J.J. Zhang, M. Qiao, H.J. Liu, J.H. Qu, Enhanced photoelectrocatalytic decomposition of copper cyanide complexes and simultaneous recovery of copper with a $Bi_2MoO_6$ electrode under visible light by $EDTA/K_4P_2O_7$. Environ. Sci. Technol. **49**(7), 4567–4574 (2015). doi:10.1021/es5062374
31. L. Liu, R. Li, Y. Liu, J. Zhang, Simultaneous degradation of loxacin and recovery of Cu(II) by photoelectrocatalysis with highly ordered $TiO_2$ nanotubes. J. Hazard. Mater. **308**, 264–275 (2016). doi:10.1016/j.jhazmat.2016.01.046
32. A.G. Munoz, Semiconducting properties of self-organized $TiO_2$ nanotubes. Electrochim. Acta **52**(12), 4167–4176 (2007). doi:10.1016/j.electacta.2006.11.035
33. J. Kruger, R. Plass, M. Gratzel, P.J. Cameron, L.M. Peter, Charge transport and back reaction in solid-state dye-sensitized solar cells: a study using intensity-modulated photovoltage and photocurrent spectroscopy. J. Phys. Chem. B **107**(31), 7536–7539 (2003). doi:10.1021/jp0348777